Wetting and domain-growth kinetics in confined geometries

Liza Monette
Corporate Research Science Laboratory, Exxon Research and Engineering Company, Annandale, New Jersey 08801

Andrea J. Liu
Department of Chemistry and Nuclear Engineering, University of California, Santa Barbara, California 93106 and Corporate Research Science Laboratory, Exxon Research and Engineering Company, Annandale, New Jersey 08801

Gary S. Grest
Corporate Research Science Laboratory, Exxon Research and Engineering Company, Annandale, New Jersey 08801
(Received 16 April 1992)

In this paper, we review the theoretical and experimental progress in understanding the controversial phase behavior of binary liquids in dense porous media. Experimental observation of metastability and hysteresis in the phase-separation behavior has led to two widely different theoretical interpretations: the random-field Ising picture and the single-pore picture. We argue that the random-field model is inapplicable to binary liquids in low-porosity media such as Vycor, and discuss the available experimental evidence on such systems. Next, we present Monte Carlo studies of phase-separation kinetics of an Ising model in a pore. We find that the domain-growth kinetics slow down dramatically once the domain size becomes comparable to the pore size, as predicted by the single-pore model. In addition, we examine the influence of temperature and interfacial phase transitions on the kinetics, and show that the domain-growth rate slows down as the temperature moves further into the two-phase region. Finally, our results for small pores, only 20 spins across, suggest that macroscopic descriptions are surprisingly successful, even at short length scales.

PACS number(s): 64.60.−i, 68.45.Gd, 47.55.Mh

I. INTRODUCTION

The phase-separation kinetics of binary liquid mixtures are completely altered when they are imbibed in porous media. Binary liquids display Ising-like phase behavior; in bulk, they are observed to separate, below the critical mixing point, into two domains, one of each phase. This is known as macroscopic phase separation. By contrast, in porous glasses such as Vycor, the two phases do not separate completely. Instead, they form many small domains, even well inside the coexistence region [1–6]. The reason for this lack of macroscopic phase separation is controversial. One possibility is that randomness of the pore structure gives rise to random-field Ising-like behavior near the critical point [7–12], which may lead to a low-temperature phase with small domains [13]. We will argue below that this picture is unlikely to apply to porous media such as Vycor. Our view, on the other hand, is based on a single-pore model with no randomness. According to this picture, confinement in a small pore slows down domain growth in certain regions of the wetting phase diagram. Therefore, macroscopic phase separation is not observed because the kinetics are too slow [14]. To date, there has been no explicit comparison of the two models. Indeed, there is surprisingly little discussion in the literature of why the random-field model might be expected to apply to two-phase systems in porous media. We attempt to fill the gap with a detailed discussion of the assumptions underlying the random-field interpretation. We also review the experimental results on binary liquids in Vycor.

In the second part of this paper, we describe Monte Carlo simulation results on the phase-separation kinetics of the Ising model in a pore. In a porous medium like Vycor, the tortuous and interconnected nature of the geometry will certainly create barriers to domain growth. [These are not the same as the energy barriers incorporated in the random-field Ising model (RFIM) picture.] The single-pore model ignores these barriers and therefore cannot provide a completely realistic description of the phase-separation kinetics in porous glass. However, the single-pore picture does yield insight into the phase-separation process by allowing one to isolate the effects of wetting. We study three main aspects of the kinetics: early-stage domain growth from the disordered state, the breakup kinetics of the tube configuration, and late-stage domain growth. Our results show that domain growth slows down dramatically once the domain size becomes comparable to the pore size. Thus, even in a system with no randomness, macroscopic phase separation is extremely slow, owing to confinement. In addition, we interpret our simulation results in terms of macroscopic constructs such as interface interaction potentials, wetting potentials, and surface tension. Earlier simulations by Liu and Grest [15] demonstrated the utility of macroscopic descriptions of *equilibrium* phase behavior in pores roughly equivalent to 60 Å in diameter. The simulations presented here indicate that macroscopic descriptions are also surprisingly successful in describing the *kinetics* of phase separation in extremely small pores.

A. Organization of paper

The rest of this introductory section is devoted to a detailed comparison between the RFIM picture and the single-pore description of binary liquids in Vycor. Some preliminary remarks on the applicability of the two models are made in Sec. I B. In Sec. I C, we summarize the argument for why RFIM behavior might be observed on approach to T_c from the single-phase region. To our knowledge, the most detailed argument was given by Andelman and Joanny.[9] We paraphrase their argument for the case of fixed composition. We conclude this subsection with a list of reasons why we believe that the RFIM picture is *inapplicable* to the experiments performed on binary liquids in Vycor.

In Sec. I D, we summarize the single-pore model. The thermodynamic phase behavior predicted by the phenomenological single-pore model of Liu and co-workers [14] has been confirmed by Monte Carlo simulations by Liu and Grest [15]. Section I E contains a review of experimental results on binary liquids in Vycor. We show that the single-pore model is more successful than the RFIM picture in capturing observed features of the phase behavior.

In Sec. II through Sec. V, we turn to the main topic of the paper, which is the kinetics of phase separation. We first review the two main features of phase separation in pores discussed in Ref. [14]. The first is the kinetics of the breakup of the tube configuration and the second is the kinetics of domain growth. The predictions of Ref. [14] were based on phenomenological arguments and hydrodynamic calculations; the details of these are summarized in Appendixes A–C.

The results in this paper are based on Monte Carlo simulations of the phase-separation kinetics of an Ising model in a single pore. The simulation model and method are described in Sec. III. The results are presented in Sec. IV. Section V contains a summary of results. We find that the kinetic behavior is quite rich, showing many features not included in the phenomenological model.

B. Random-field model versus single-pore model: Preliminary remarks

Before describing the two models in detail, we must specify the geometries of the porous media under consideration. It is useful to draw a distinction between materials like Vycor [16], which have fairly low porosities (roughly 30%), and materials such as aerogels [17] or other silica gels [18], which have high porosities (over 90%). Such gels resemble a dilute network of strands, and probably cannot be described by a single-pore model. Thus, the conclusions of this paper, which are based on the single-pore picture, apply only to dense porous media. We will argue below that it is unlikely that the random geometry in low-porosity materials such as Vycor will lead to random-field Ising behavior. It is possible, however, that low-density porous media may exhibit random-field behavior [19,20].

We must also address the role of the constraint of constant composition. This constraint, equivalent to the canonical ensemble, applies to most experiments on binary liquids in porous media [2,3,5,6,20,21]. It is also applicable to vapor-liquid experiments at fixed density [22]. In the experiments, the samples were typically prepared in the single-phase region, by soaking the porous glass in a bath rich in the nonwetting component, so that the mixture inside would be critical. Almost all of the supernatant liquid was then poured off. In principle, the fluid inside the porous medium could change in composition by ejecting the unwanted component from the sample; on the time scale of the experiment, however, the composition inside was fixed [4]. Thus, the experimental conditions correspond to the canonical ensemble.

Wetting phenomena inside confined geometries such as pores have long been overlooked because previous theoretical work has focused on the case where the system is in contact with a reservoir at the same chemical potential; this corresponds to the grand canonical ensemble. In this case, capillary condensation occurs near the critical point; the pore fills with a single phase rich in the wetting component. The phenomenon of capillary condensation has been well studied both theoretically [23,24] and experimentally [25,26].

In the single-pore model, we have chosen to work in the canonical ensemble for direct comparison with the experiments. However, we could equally have chosen to use the grand canonical ensemble, with a chemical potential that varies with temperature in such a way that the composition inside is always the same. Since both pictures are equivalent, the wetting transitions that we predict should also occur in the grand canonical ensemble. We suspect that these transitions were not discovered previously because they occur far from the critical point, when the chemical potential strongly favors the nonwetting phase.

By the same token, our predicted behavior should be seen in liquid-vapor systems confined in Vycor at low pressures. Heat capacity and vapor-pressure isotherm measurements of Wong [27] on liquid-vapor ^{4}He in Vycor indicate that there is no sharp phase transition. We suggest that this is consistent with the finite-size rounded and shifted transition expected in the single-pore model.

C. Random-field model

The interpretation of a binary liquid in a porous medium as a random-field Ising model (RFIM) was introduced by Brochard and de Gennes in 1983 [7,8]. We will not attempt to review the substantial theoretical literature on the RFIM or to discuss recent theoretical work on the RFIM motivated by experiments in porous media [11,12]. Rather, we will focus on the question of why the RFIM might be applicable to Ising-like systems in porous media. The argument was most clearly stated by Andelman and Joanny [9]. Here, we adapt their argument to the case of constant composition. Note that the RFIM picture has also been applied to a different class of problems involving *displacement* of one fluid by another in a porous medium [7]; an excellent critique of such approaches to imbibition problems was provided by Bruinsma [28].

Label the two components of a binary liquid mixture A and B and let the pore surface prefer A. Assume that the composition inside the porous medium is fixed, and let the average pore radius be r_0. Now divide the porous medium into cells r_0 on a side, and denote the surface-to-volume ratio in cell i by A_i. Then A_i is a random variable. When A_i is large, more of component A is pulled to the surface, leaving more B in the bulk. This comparison shift towards B can be considered a result of a field acting on cell i. Thus there are random fields h_i on the scale of the pore size. Now, if the correlation length for the binary liquid is larger than the cell size, then one can coarse-grain the system so that each cell now represents a site. The system should then be describable by the random-field Ising model. Thus, this picture predicts random-field-like behavior in a region surrounding the bulk critical point.

Note that the RFIM description assumes that the fluid can be divided into two parts: an adsorption layer of A which is "immobilized" in the sense that it does not participate in critical fluctuations, and a "free fluid," namely the remaining fluid, which does participate in critical fluctuations. The RFIM picture applies to the free fluid, in that the random fields are applied to the free fluid only. Frisken, Ferri, and Cannell [20] show that the concept of a free fluid is valid for binary liquids in dilute silica gels. We stress, however, that the gradient free energy between the immobilized layer and the free fluid is not explicitly included in the RFIM picture. Recent results of Frisken and Cannell [21] suggest that the gradient free energy may play a crucial role in the phase behavior of binary liquids in dilute gels.

There are several reasons why it is unlikely that the RFIM picture, as stated above, is applicable to binary liquids in Vycor. The first has to do with the magnitude of the average composition shift of the free fluid due to the average value of the field $\langle h_i \rangle$. Frisken, Ferri, and Cannell [20] have measured the average composition shift in dilute silica gels, and have shown that these can be substantial near the critical point. It is reasonable to suppose that Vycor, having a much lower porosity than the gels, should give rise to much larger composition shifts. Raman-scattering results by Dierker, Dennis, and Wiltzius [4] on Lutidine and water in Vycor in contact with a bath of the mixture suggest that the composition shifts are indeed quite large. In fact, the composition shift in the free fluid in Vycor should be roughly comparable to the shift in the immobilized, adsorbed A-rich fluid at the wall. Thus, the free fluid may be shifted so strongly towards B that is is equally immobilized. In this case, the RFIM picture would no longer be useful. In addition, the correlation length in the free fluid would be quite short, so that the limit $\xi \gg r_0$ required by the RFIM picture would not be achievable.

Dierker and co-workers [29,3] have suggested a more subtle scenario by which RFIM behavior might arise in Vycor. As discussed above, the composition differences between the adsorbed fluid and the free fluid increase as the critical temperature is approached from the single-phase region. This leads to large gradients in composition, since the composition must change from A-rich near the wall to B-rich in the center of the pore. At a certain point, the system may undergo a "pseudowetting" transition to a "pseudoplug" configuration, where the gradients now run along the pore length rather than across the pore. Note that Wiltzius, Dierker, and Dennis [3] refer to this as a "finite-size wetting transition." This is a misleading name, since they believe it occurs in the single-phase region. Based on their static and dynamic light-scattering results for Lutidine and water in Vycor, Wiltzius, Dierker, and Dennis [3] suggest that this "pseudowetting" transition occurs 8° from the bulk critical point in what would ordinarily be the two-phase region in the bulk mixture, but which they propose is still the single-phase region in Vycor. Once the system has undergone this transition to "pseudopartial wetting," the correlation length might grow to encompass many pore sizes. The system might therefore cross over to RFIM behavior. This is an interesting possibility, which may account for their static and dynamic light-scattering results, but appears inconsistent with recent neutron-scattering results of Lin *et al.* [6]. (See Sec. I E below.)

The second difficulty in applying the RFIM picture to binary liquids in porous media is that the average value of the field $\langle h_i \rangle$ may exceed the root-mean-square deviation in the field $(\langle h_i^2 \rangle)^{1/2}$. In fact, if the binary liquid mixture inside the porous medium is at critical composition, all of the composition shifts will be towards enhanced B, so all the random fields have the same sign. In this case, there is no frustration, because both the fields h_i and the interaction energy $J \equiv E_{AA} + E_{BB} - 2E_{AB}$ favor B in the free volume. This point has also been stressed by Maritan and co-workers [11]. In order to see metastability, therefore, the composition inside the medium must be sufficiently A rich so that $\langle h_i \rangle < (\langle h_i^2 \rangle)^{1/2}$. Even if the composition is sufficiently rich in A, however, the condition $\langle h_i \rangle = 0$ is only satisfied at one temperature, since the amount of A attracted to the surface varies with temperature. The effect of temperature on $\langle h_i \rangle$, or the average composition shift, has been elegantly illustrated in experiments by Frisken, Ferri, and Cannell on Lutidine-water [20] and by Frisken and Cannell on isobutyric acid–water [21] mixtures in dilute silica gels. (As noted in the preceding paragraph, $\langle h_i \rangle$ should be even larger in Vycor, where the surface area to free volume ratio is higher.) Most of the Vycor experiments have been carried out at critical composition [2,5,6], so one would not expect metastability to arise from the random fields.

Finally, we note that in a dense porous medium like Vycor, crossover to one-dimensional Ising behavior may preempt crossover to RFIM behavior. In Vycor, the distance between junctions is comparable to the pore radius. According to recent experiments by Levitz *et al.* [16], the persistent length of the pores is about $l = 45$ Å, while the average radius is $r_0 = 35$ Å. One would expect the system to cross over to $d = 1$ behavior when the correlation length ξ becomes comparable to r_0. On the other hand, the system should cross over to the RFIM when ξ becomes comparable to the distance between pore junctions, l. If $r_0 \ll l$, then crossover to $d = 1$ behavior will occur first, the correlation length will never exceed r_0 by

more than a factor of order unity, and the system will never cross over to RFIM behavior. Since r_0 and l are comparable in Vycor, it is unlikely that a clean crossover to RFIM behavior could be observable.

D. Single-pore model

The single-pore description for a binary liquid in Vycor was introduced by Liu, Durian, Herbolzheimer, and Safran [14]. The resulting equilibrium wetting-phase diagram is shown in Fig. 1; the shape of the diagram has been confirmed by recent Monte Carlo simulations by Liu and Grest for a lattice-gas model [15]. In this model, the binary liquid mixture is confined in a single cylindrical pore. For simplicity, we assume that the mixture is of critical composition. The system undergoes a transition from a single mixed phase to two coexisting phases, α and β, one rich in A molecules and the other rich in B molecules, as the temperature is varied through an Ising-like critical point. This transition (not shown in Fig. 1) is rounded and shifted from the bulk critical point due to the finite radius of the pore. Near the critical point in the two-phase region, the wetting phase α will coat the pore, and the nonwetting phase forms a concentric inner cylinder; this is the "tube" configuration (see Fig. 1). Since the surface prefers α, there is a free-energy cost per unit area, or wetting potential, $V(r)$, on the $\alpha\beta$ interface, pushing it towards the center of the pore. This is balanced by the $\alpha\beta$ interfacial tension. Since the composition is held fixed, the amount of each phase is also fixed for a given temperature. Under conditions of fixed volume, the interfacial tension gives rise to an outward pressure, pushing the interface away from the pore center. Now consider what happens as a function of reduced temperature $t=(T-T_c)/T_c$. As $|t|$ increases, the interfacial tension $\sigma_{\alpha\beta}$ increases as $|t|^{\mu}$, where $\mu=2\nu\approx 1.26$ for the $d=3$ Ising model [30]. The wetting

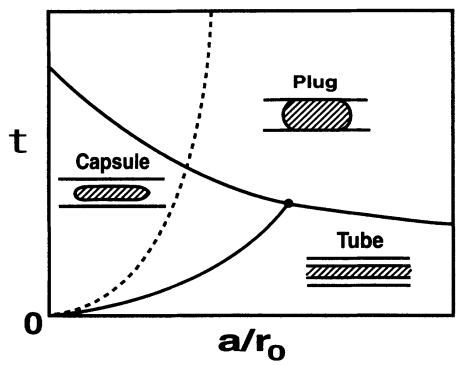

FIG. 1. Wetting-phase diagram in a pore of radius r_0, showing the tube, capsule, and plug configurations. For the parameters typically used in our simulations ($J_1/J=1$, $H/J=0$, and $H_1/J=0.7$), the wetting transition between the plug and the capsule or tube phases is second order, and the interfacial shape transition between the capsule and tube phases is first order. The dashed line represents the "spinodal line" of the tube configuration; the tube is metastable between the spinodal line and the interfacial shape transition, and unstable beyond the spinodal line.

potential also increases, because the difference in composition between the phases increases. Thus, $V(r)$ increases as $|t|^{\beta}$, where $\beta\approx 0.33$. Clearly, $\sigma_{\alpha\beta}$ increases more rapidly than $V(r)$ with $|t|$, leading to a decrease in the wetting-layer thickness. Since the total volume of each phase is fixed at critical composition, the system may undergo a first-order transition to a "capsule" configuration as the wetting-layer thickness decreases. We call this an interfacial shape transition. As $|t|$ is increased still further, the system may eventually undergo a second transition to a "plug" state, where the interface stretches across the pore to reduce the total interfacial area. This is the analogue of the wetting transition at a planar surface [31–33]. A recent exact calculation of the planar Ising model in a finite-size strip by Abraham, Svrakic, and Upton [34] supports the existence of the wetting transition in a confined geometry. They apply the Wulff construction to bond-energy correlation functions to demonstrate the possible domain-wall configurations, and obtain the capsule and plug configurations. Note that the plugs in their Fig. 1(d) are slightly misdrawn; the interface should make the contact angle ϑ_c, with *both* walls, rather than ϑ_c at one wall and $\pi-\vartheta_c$ at the other wall.

The phase behavior of Ising systems has also been studied in other regular confined geometries. For example, the behavior of Ising systems confined between parallel plates has been studied by Nakanishi and Fisher [35], and more recently, by Parry and Evans [36] and Swift, Owczarek, and Indekeu [37]. Nakanishi and Fisher [35] examined the case most analogous to the pore, where the two plates have equal surface fields. In contrast to the pore results, however, they did not observe a wetting transition between the plates. We believe that they did not see the wetting transition because they employed different boundary conditions. They used a zero-slope boundary condition at the plates, which is valid for strong fields sufficiently close to the critical point. Liu and co-workers [14], on the other hand, implicitly used the wetting boundary condition, where the slope of the concentration at the surface is related to the surface field. This wetting boundary condition was used by Nakanishi and Fisher to study wetting transitions against a single planar surface [31].

Recently, Parry and Evans [36] and Swift, Owczarek, and Indekeu [37] have considered the parallel-plate geometry with *opposing* surface fields on the two plates. Here, capillary condensation is suppressed by applying opposite-surface fields, so the behavior in the two-phase region can easily be studied. The results of Swift, Owczarek, and Indekeu [37] are qualitatively similar to ours; there is a tubelike configuration, where the interface lies halfway between the plates; and there is a pluglike configuration, where the two phases are separated by interfaces stretching between the plates. There is no capsule phase in their model because the complete-wetting interface position is fixed in the center of the gap by symmetry. In addition, Swift, Owczarek, and Indekeu [37] have shown that the wetting transition can be first order, critical, or tricritical, and that the transition merges smoothly into the planar wetting transition as the plate spacing diverges. These results are consistent with the

simulation results of Liu and Grest for cylindrical pores at constant composition [15].

One of the insights provided by the single-pore model is that it is difficult for the system to reach equilibrium [14]. For example, if the system is quenched from the single-phase region into the two-phase region, it will form into many short capsules or plugs, instead of one long capsule or plug. If these capsules or plugs are formed by nucleation or spinodal decomposition, we would expect the length of the resulting capsules and plugs to be on the order of the pore radius. Once these short capsules or plugs are formed, Liu *et al.* [14] argued that the kinetics of domain growth slow down drastically, thus prohibiting macroscopic phase separation. This process will be described in more detail in Sec. II.

In a true porous medium like Vycor, there are pore junctions and variations in the pore radius. Nevertheless, we suggest that there are analogues to the three configurations found in cylindrical pores. These analogues are depicted in Fig. 2. The tube configuration corresponds to a bicontinuous phase where both phases percolate through all of the pores. The capsule configuration corresponds to a percolating layer of the α phase coating all of the pore surface, interspersed with droplets of the nonwetting phase at the junctions of pores. Plugs correspond to alternating domains of the two phases separated by interfaces stretching across the pore cross section. The transitions between the three configurations will be shifted and rounded owing to geometrical irregularities, but should still be governed by the competition between surface tension and wetting forces.

Numerical simulations have recently been carried out by two groups, Lee [38] and Chakrabarti [39], on more realistic model porous media in two dimensions, to study the kinetics of domain growth. Lee used Monte Carlo simulation to study phase separation in a system with roughly parallel walls with irregular gaps. He found that the domain growth exhibits scaling behavior in certain regimes, and obeys a $t^{1/3}$ growth law when the *minimum* distance is used to measure the correlation function instead of the usual *Pythagorean* distance [38]. Chakrabarti first used a cell-dynamics scheme to simulate a two-dimensional spinodal decomposition pattern as model Vycor. He then numerically integrated the Cahn-Hilliard equation with appropriate boundary conditions at the pore walls. He found that domain growth slows down dramatically when the average domain size grows to be comparable to the average pore radius. These results for model Vycor support the single-pore picture [39].

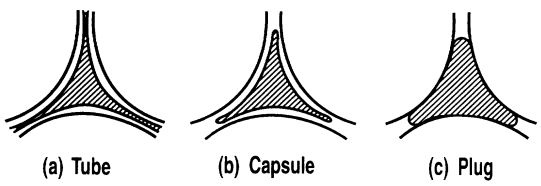

FIG. 2. Schematic drawing of a pore junction in a porous medium like Vycor, showing the analogues of the (a) tube, (b) capsule, and (c) plug configurations.

E. Experiments

There have been several experiments on binary liquid mixtures in porous glasses. The first was static light scattering at 90° performed by Goh, Goldburg, and Knobler [1] on hexane and perfluorohexane in a glass with an average pore size of 45 nm. Their results were consistent with extremely slow phase separation in the pores, in a temperature regime quite *far* from T_c, where the correlation length should be much shorter than the pore size of 45 nm. Thus, the RFIM picture is not expected to apply, and their conclusions are consistent with the single-pore picture.

We now turn to a set of experiments on 2,6-Lutidine and water in Vycor. This mixture has an *inverted* coexistence curve with $T_c^0 = 33°\,\mathrm{C}$ and $\phi_L^c = 0.3$, where ϕ_L is the volume fraction of Lutidine, and Lutidine wets the Vycor. Dierker and Wiltzius [2] and Wiltzius, Dierker, and Dennis [3] made static and dynamic light-scattering measurements and found evidence for a "pseudowetting" transition 8° above the bulk T_c^0, in what they suggest is still the single-phase region. As discussed in Sec. I C, the system reduces its gradient free energy by developing gradients along the pore length, rather than across the pore width. Between 8° C and 30° C above T_c^0, Dierker and Wiltzius [2] propose that the system remains in the single-phase region with a steadily increasing correlation length. Finally, the system reaches a history-dependent frozen-domain state at about 30° C above the bulk-critical temperature. They interpreted this temperature as the random-field transition temperature. Their interpretation will be discussed further below. We should note here that we have not yet calculated the autocorrelation function within the single-pore model to interpret the dynamic light-scattering results. It is possible that diffusive motion of the capsules may give rise to the relaxation times they observe.

The two most recent experiments by Dierker and Wiltzius (DW) [5] and by Lin, Sinha, Drake, Wu, and Thiyagarajan [6], both use small-angle neutron scattering to study Lutidine and water in Vycor. The average composition inside the pore is adjusted to be both critical and contrast-matched to the Vycor by using a mixture of H_2O, D_2O, and Lutidine. The data from the two experiments appear at least qualitatively similar, but the data analyses and interpretations differ in some respects. DW conclude that their data are consistent with the RFIM picture, but do not rule out the single-pore picture. Lin *et al.* conclude that their data support the single-pore picture. To understand the differences, we must examine the two interpretations underlying the data analyses.

The DW interpretation is based on the same picture they used to analyze the static and dynamic light scattering. Below T_c^0, the system is in the single-phase region and exhibits the expected three-dimensional Ising behavior. Thus the scattering intensity $S(q)$ can be fitted with a Lorentzian form:

$$S(q)=\frac{A_1}{1+q^2\xi_1^2} \quad (T<T_c^0) . \tag{1.1}$$

Above T_c^0, DW assume that the system *does not* phase separate, but begins to cross over to RFIM behavior. Thus, correlations in the fluid composition due to the random fields begin to develop, and a Lorentzian-squared term appears in $S(q)$ [40]. (DW also noted that their Lorentzian-squared term could arise from microdomains rather than from random fields, as discussed in more detail below.) Finally, DW include a q-independent term due to background incoherent scattering. So the expected form for $S(q)$ is

$$S(q)=A_0+\frac{A_1}{1+q^2\xi_1^2}+\frac{A_2}{(1+q^2\xi_2^2)^2} \quad (T_c^0<T<T_{\rm rf}) . \tag{1.2}$$

Since the system is still in the single-phase region, the only length scale present is still the correlation length, so we should have $\xi_1=\xi_2=\xi$. DW found that best fits were obtained for ξ_1 and ξ_2 comparable in value. At $T=T_{\rm rf}\sim 60^\circ$C, DW suggest that the system goes through the random-field transition to an ordered random-field state, with no change in the expected form $S(q)$.

This picture describes the data well, with one crucial caveat. There is a residual peak in the data at significantly higher q than the Vycor structure peak at $q\approx 0.02$ Å^{-1}. In the data of Lin *et al.*, the extra peak occurs at $q\approx 0.03$ Å^{-1}. In the DW analysis, an *ad hoc* Gaussian term of the form $A_p\exp[-(q-q_p)^2/\mu^2]$ is introduced to account for this peak. The amplitude of the peak A_p is found to increase as T increases above T_c^0 [29]. The actual form used to fit $S(q)$ is therefore [41]

$$S(q)= A_0+\frac{A_1}{1+q^2\xi_1^2}+\frac{A_2}{(1+q^2\xi_2^2)^2} + A_p\exp[-(q-q_p)^2/\mu^2] \quad (T_c^0<T<T_{\rm rf}) . \tag{1.3}$$

The main difference in the analyses of DW and Lin *et al.* lies in the interpretation of this peak. According to the picture of Lin *et al.*, this peak is due to the presence of a wetting layer, which introduces structure on a scale smaller than that of the pore size, and hence a peak at higher q than the Vycor structure. Below T_c^0, Lin *et al.* interpret their data using Eq. (1.1), as did DW. Above T_c^0, however, they assume that the system is in the two-phase region. The two phases form microdomains on the scale ξ_2. Debye, Anderson, and Brumberger [42] showed in 1957 that the form of $S(q)$ for a system with alternating domains of two phases is a Lorentzian-squared term, where the amplitude A_2 describes the contrast between the two phases and the length scale ξ_2 derives from the domain size. In the high-q limit, the Lorentzian-squared term reduces to Porod's law: $S(q)\sim q^{-4}$. In principle, there is also a Lorentzian, or Ornstein-Zernike term, arising from fluctuations in the usual manner. However, in the temperature regime of the experiments, the correlation length ξ_1 is short compared to the pore size, and the Lorentzian term is approximately a constant. Thus, Lin *et al.* fit their data to the form

$$S(q)=A_0+\frac{A_2}{(1+q^2\xi_2^2)^2}+A_3S_{\rm skin}(q,\Delta) \quad (T>T_c^0) , \tag{1.4}$$

where $S_{\rm skin}(q,\Delta)$ is the structure factor for Vycor coated with a contrasting wetting layer of thickness Δ. Sinha [43] has shown that $S_{\rm skin}$ can be related analytically to a chord distribution which characterizes the structure of empty Vycor. When this term is incorporated, it appears to account for the peak also seen by DW at $q\sim 0.05$ Å^{-1}. The increase in amplitude of this peak with T implies that the contrast between the wetting layer and the Vycor increases. This is consistent with phase separation on the pore scale, where the wetting layer grows richer in Lutidine as the temperature moves away from criticality.

Apart from the peak, the two analyses yield consistent results. Both analyses show that there is clear evidence of increased contrast between the wetting layer and the Vycor as T increases above T_c^0. This is consistent with moving *away* from criticality, further into the two-phase region. Finally, it is important to note that, according to both data analyses, the correlation length ξ_1 never exceeds the pore diameter. Thus, it is likely that the system never crosses over to the RFIM limit, because critical fluctuations are suppressed by the finite pore size. We believe that a reasonable explanation is that the crossover to RFIM behavior is preempted by crossover to one-dimensional Ising behavior, as discussed in Sec. I C.

To summarize the neutron-scattering results, the interpretation of Lin *et al.* appears to explain all of the data, including the peak not accounted for in the DW analysis. In the analysis of Lin *et al.*, the peak arises naturally, owing to the presence of a wetting layer. It is difficult to understand why a wetting layer, or strong composition gradient, should arise in the RFIM picture in this regime. Indeed, according to the static and dynamic light-scattering results of Wiltzius, Dierker, and Dennis [3], the system should be a "pseudo-partial-wetting" regime with *no* wetting layer. Thus the RFIM picture is inconsistent with the results of the analysis of Lin *et al.*

II. KINETICS OF PHASE SEPARATION IN PORES

According to the single-pore model, the kinetics of phase separation lie at the core of the unusual behavior observed in binary liquids in porous media. There are two main features of the kinetics that we wish to explore in detail in this paper. Both of these were discussed in Ref. [14]; the first is the breakup of the tube configuration when quenched into the capsule or plug regimes, and the second is the unusually slow domain-growth kinetics in the capsule and plug regimes. This section contains a summary of the behavior predicted in Ref. [14] on the basis of hydrodynamic arguments. We end this section with a list of factors not discussed in Ref. [14], which might influence the kinetic behavior, and which can be examined with simulations.

A. Breakup kinetics of tube

Simulations by Liu and Grest [15] show that the interfacial shape transition between the tube configuration and the capsule or plug configurations is a first-order transition. In this section, we discuss the kinetics associated with quenches from temperatures above to below this transition. In other words, we study how the tube breaks up into capsules or plugs when it is quenched into the capsule or plug regimes. In an earlier paper [14], we predicted that the tube can break up into capsules or plugs via a Rayleigh-like instability. This instability occurs for energetic reasons; the system can reduce its surface area by allowing long-wavelength perturbations of the tube radius. A simple energetic argument, summarized in Appendix A, shows that there is a line in the phase diagram as a function of temperature and pore size beyond which the tube is unstable. This line, which is analogous to a spinodal line, always lies at temperatures below the interfacial shape-transition line (see Fig. 1). Thus the phenomenological theory predicts a nucleation regime, lying between the transition line and the spinodal line, where the tube can break up into a capsule by a nucleation, or pinching-off event. The theory also predicts a spinodal regime, lying below the spinodal line, where the tube breaks up via a Rayleigh-like instability. In Appendix B, we present a linear stability analysis for the breakup based on the Navier-Stokes equation with a wetting force. Since the instability is energetic in origin, however, it should occur even if there are no hydrodynamics in the system. Thus, it should occur in our Ising model simulations with Kawasaki dynamics, which include diffusion but not hydrodynamics. Our simulation results for the breakup kinetics of the tube are presented in Sec. IV B.

B. Domain growth kinetics

The kinetics of domain growth have been studied extensively in bulk Ising-like systems [44]. When a binary fluid mixture is rapidly quenched from above to below the coexistence curve, the system relaxes either via nucleation or spinodal decomposition. In the late stages of both nucleation and spinodal decomposition, the domain size grows with time as $r \sim t^{1/3}$. In this regime, coarsening is driven by a pressure difference between larger and smaller domains. Each domain is under a Laplace pressure σ/r, where σ is the interfacial tension and r is the domain radius. Thus, smaller droplets are under larger pressure, which drives diffusion from the smaller droplets to larger ones.

Domain growth in a cylindrical pore follows a very different course. In an earlier paper, we discussed why coarsening in confined geometries is expected to be unusually slow [14]. As mentioned above, in the early stages, domains can form and grow via nucleation or spinodal decomposition, as in the bulk. When the domain size becomes comparable to the pore radius, however, the coarsening process slows down dramatically. Once the domains have formed into short plugs or capsules, the mechanism of Ostwald ripening is severely inhibited because the curvatures of the end caps of the plugs or capsules are nearly independent of their length. Thus, short and long plugs are under the same Laplace pressure, and there is no driving force for diffusion from short plugs to long ones. Similarly, there is no Ostwald ripening of capsules. However, an individual capsule can diffuse as a whole and may coalesce with a neighboring capsule. In order for the capsule to move, however, the wetting phase must flow through the wetting layer, because the liquids are incompressible. Thus, the capsule diffuses more slowly if the wetting layer is thinner. By similar reasoning, plugs do not diffuse at all. A simple hydrodynamic calculation of the capsule diffusion constant as a function of wetting-layer thickness is summarized in Appendix C.

C. Need for simulations

In the next section, we present results of Monte Carlo simulations of the Ising model at fixed composition. With the simulations, we can study many factors that could influence domain growth. First, the first-order interfacial shape transition from the capsule to the tube phase can influence the kinetics, because the system can be trapped in metastable states. Second, attractive interactions between interfaces can lead to domain growth. In the Ising model, these interactions are short-ranged and decay exponentially with the correlation length. Third, we note that for binary liquids in pores, the kinetics are governed by diffusion as well as hydrodynamics. In the hydrodynamic calculations presented in Appendixes B and C, diffusion is ignored. It is valuable to study the transport-mechanism dependence by simulating the Ising model with Kawasaki dynamics, where the kinetics are governed by diffusion only. Finally, the phenomenological calculations are based on macroscopic considerations, and it is not clear whether they apply in the 60-Å pores found in Vycor. Clearly, simulations in small pores provide a stringent test of the validity of the macroscopic picture.

III. SIMULATION MODEL

In the simulations, we employ the standard mapping of a binary liquid mixture with molecular species A and B onto a lattice-gas model with spin orientations $\sigma_i = \pm 1$, governed by the following Hamiltonian:

$$\mathcal{H} = -J \sum_{\text{bulk}\langle i,j\rangle} \sigma_i \sigma_j - J_1 \sum_{\text{surface}\langle i,j\rangle} \sigma_i \sigma_j - H_1 \sum_{\text{surfaces}\langle i,j\rangle} \sigma_i \ , \tag{3.1}$$

where J is the coupling between bulk spins, J_1 is the coupling between surface spins, and H_1 is the surface field. In this model, we impose short-ranged wetting forces; i.e., the surface field H_1 only acts on the first layer of spins next to the pore wall, and the interactions between spins are restricted to nearest neighbors only. Thus, the effective interface potential, or wetting potential, decays exponentially with the correlation length. The pore is a parallelepiped of dimensions $L_\perp \times L_\perp \times L_z$, with L_z chosen such that $L_z \gg L_\perp$. We impose periodic boundary conditions in the longitudinal direction L_z. The surface

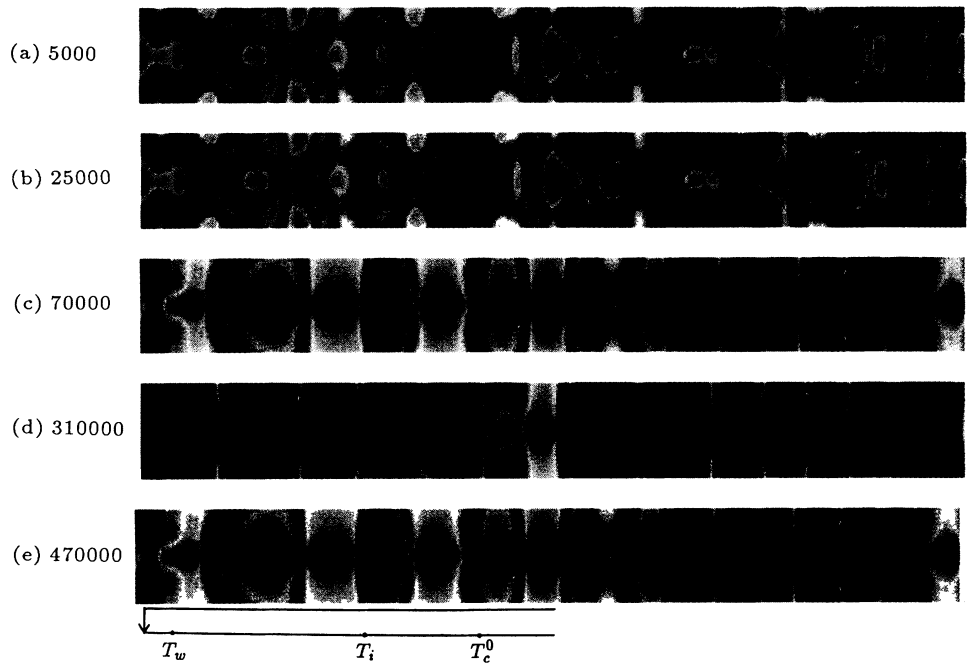

FIG. 3. Spinodal decomposition in a pore. We quench from the disordered phase ($k_BT/J=2k_BT_c/J$) into the plug phase ($k_BT/J=3.2$) at time $t=0$. The surface coupling is $J_1/J=1.0$, the bulk field is $H/J=0$, and the surface field is $H_1/J=0.1$. Magnetization profiles are shown at the times indicated on the left. The surface field is extremely low so the contact angle in (e) is nearly 90°. Note that the domain growth slows down once the domain size becomes comparable to the pore radius. These profiles were obtained by averaging over 20 000 MCS.

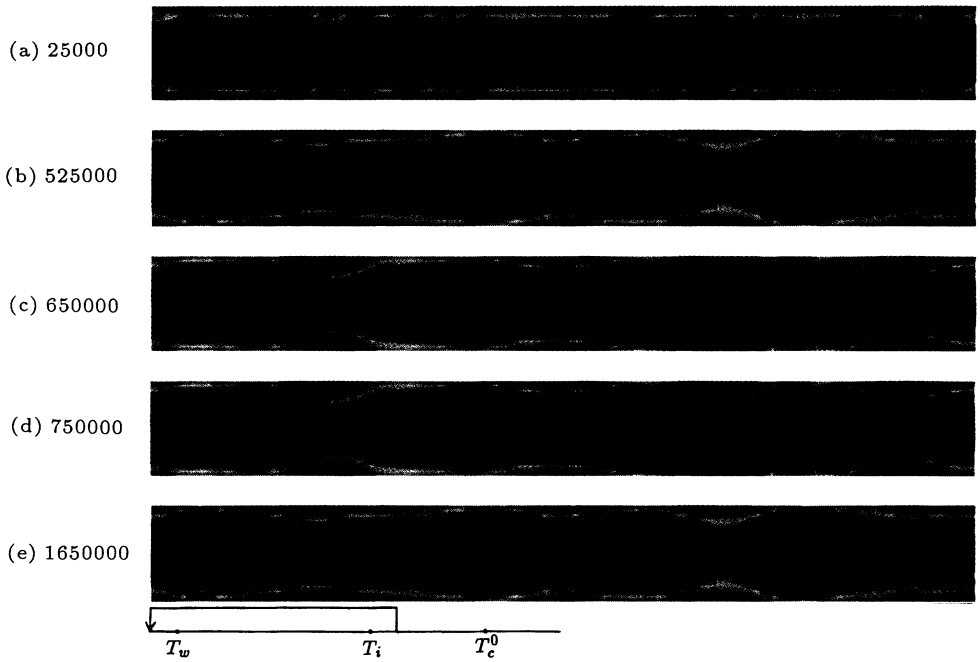

FIG. 4. Tube breakup kinetics. We quench from the tube phase ($k_BT/J=4.25$) into the plug phase ($k_BT/J=3.25$). The parameters $J_1/J=1.0$, $H/J=0$, and $H_1/J=0.7$ are used. Times are indicated on the left. Note that the tube pinches off first at one point, so it breaks up via nucleation. However, it eventually pinches off at two more points, to form three nearly equal-sized plugs, which one would expect if it had broken up via an instability ("spinodal decomposition"). Thus the evidence for the existence of a "spinodal line" is inconclusive. The profiles were obtained by averaging over 25 000 MCS.

field and surface coupling act only along the other four surfaces of the parallelepiped. All of our simulations were performed at fixed surface field $H_1/J=0.7$ and fixed surface coupling $J_1/J=1.0$, unless otherwise noted.

The three-dimensional Ising model on a simple cubic lattice has a critical point [30] at $k_BT_c/J=4.51$. All of the results presented here were obtained for the system size $L_\perp=20$ and $L_z=280$. For this size, the wetting and interfacial shape-transition temperatures were calculated in Ref. [15] to be $k_BT_w/J=3.4$ and $k_BT_i/J=4.15$, respectively. According to the results of Liu and Grest [15], the wetting transition is fairly insensitive to the pore length L_z, while the interfacial shape transition temperature varies linearly with $1/L_z$. In the limit $L_z\to\infty$, Liu and Grest found $k_BT_i/J=4.28$. Note that the typical pore diameter in Vycor is roughly 60–70 Å [16]; this is identical to our pore size $L_\perp$ if we take the lattice spacing to be the molecular size of roughly 3 Å.

In keeping with the constraint mentioned in Sec. I B, the simulations are performed in the canonical ensemble. Thus, the total magnetization is held constant; in the studies presented here, the magnetization was actually fixed at zero. For the dynamics, we chose a more efficient variation of the Kawasaki algorithm, known as pair-flip dynamics. Nearest-neighbor spins σ_i and σ_j are exchanged with the following probability:

$$p_i=\begin{cases}1 & \text{if } \sigma_i=-\sigma_j\ ,\\ 0 & \text{otherwise}\ .\end{cases} \tag{3.2}$$

The acceptance rate is given by

$$A(\{\sigma\}\to\{\sigma'\})=\min\left[1,\frac{\exp(-\beta\mathcal{H}\{\sigma'\})}{\exp(-\beta\mathcal{H}\{\sigma\})}\right], \tag{3.3}$$

where σ' represents the new spin configuration with $\sigma_i'=-\sigma_i$ and $\sigma_j'=-\sigma_j$.

The simulation results are displayed as magnetization profiles in Figs. 3–7. These profiles are obtained by averaging the magnetization over square rings, for each square cross section along the pore length L_z. For example, the four spins lying in the innermost ring of the square cross section are averaged to obtain $m(r=1,z)$ for each value of z along the pore length. Similarly, the $4(2n-1)$ spins lying in the nth ring are averaged to obtain $m(r=n,z)$, where the index n runs from $n=1$ to $n=L_\perp/2$. In cylindrical coordinates, this process is equivalent to obtaining a radial profile $m(r,z)$ by averaging over the azimuthal angle. The resulting magnetization profiles are then averaged over at least 10 000 Monte Carlo steps per spin (MCS) to obtain better statistics. This time average increases the apparent thickness of the $\alpha\beta$ interface in all our figures. The intrinsic interfacial thickness should be the bulk-correlation length, which is at most one lattice spacing in the temperature regime shown in the figures. The interfaces appear much more diffuse because of capillary waves. In a bulk three-dimensional system, the capillary waves diverge, smearing out the interface completely. In this case, however, the interface position, or wetting-layer thickness, is deter-

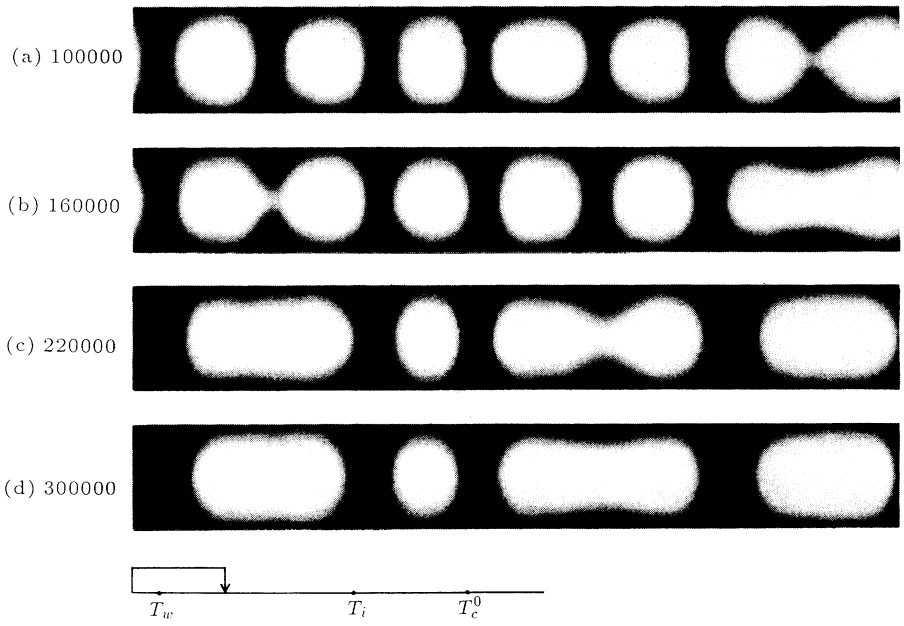

FIG. 5. Domain-growth kinetics. We heat from the plug phase ($k_BT/J=3.2$) into the capsule phase ($k_BT/J=3.55$) just above the wetting transition at time $t=0$. We use $J_1/J=1$, $H/J=0$, and $H_1/J=0.7$. The wetting layer forms quickly after the burn [see (a)], but the capsules grow extremely slowly, apparently because the interaction between interfaces is short-ranged compared to the spacing. See Figs. 6 and 7 for comparison of growth rates. Profiles were averaged over 10 000 MCS.

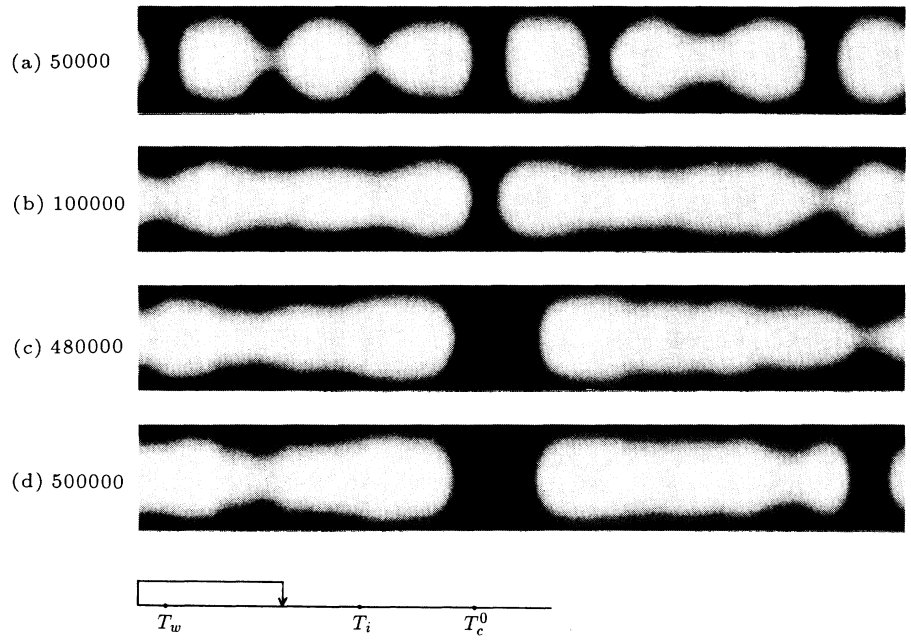

FIG. 6. Domain-growth kinetics. We heat from the plug phase ($k_BT/J=3.2$) to roughly the midpoint of the capsule phase ($k_BT/J=3.75$) at $t=0$. The coupling constants and fields are the same as in Fig. 5. The wetting layer is thicker than in Fig. 5, and the kinetics of capsule coalescence are noticeably faster. Profiles were averaged over 10 000 MCS.

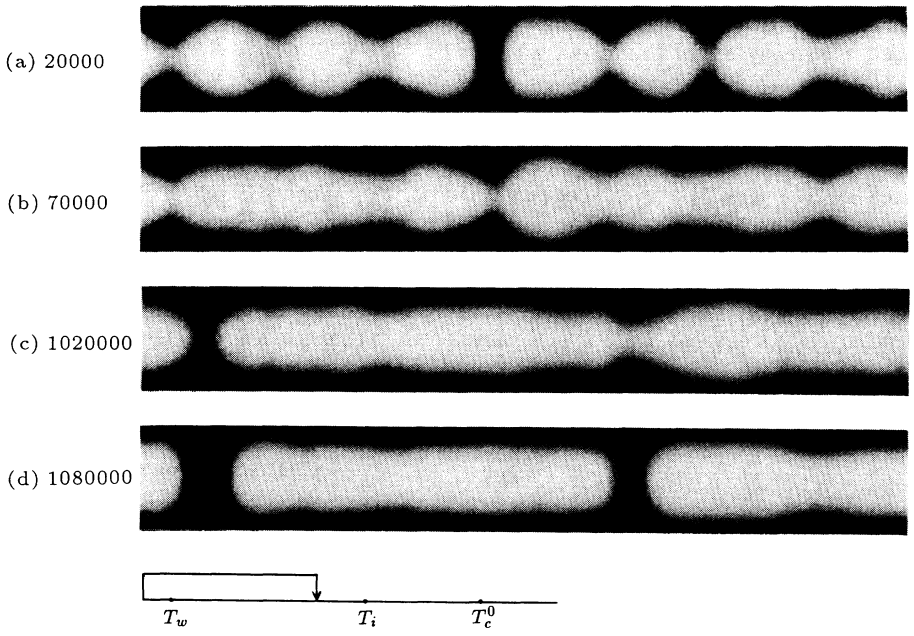

FIG. 7. Domain-growth kinetics. We heat from the plug phase ($k_BT/J=3.2$) into the capsule phase ($k_BT/J=3.85$) just below the interfacial shape transition. The coupling constants and fields are the same as in Fig. 5. The capsules coalesce rapidly [see (a)]. The influence of the nearby interfacial shape transition is apparent; the system is trapped in the metastable tube, and cannot reach the equilibrium capsule configuration until a nucleation event occurs [see (c)]. Profiles were averaged over 30 000 MCS.

mined by a minimum in the free energy due to the competition between wetting forces and interfacial tension. Thus there is an energy cost for capillary waves and the spectrum does not diverge. Averages over 10 000 MCS and over 30 000 MCS yield similar apparent interfacial thicknesses.

In Figs. 3 and 4, we have used the following color code to represent the magnetization m: $m=+1$ is red, $m=-1$ is violet, and intermediate values are given by the spectrum. In Figs. 5–7, we have used a gray scale to represent m: $m=+1$ is black and $m=-1$ is white. In all of the magnetization profile plots, we reflect the radial profiles around the z axis to obtain the depicted lengthwise pore cross sections.

Finally, in our discussion of the results, we refer to temperature *burns*; a "burn" is the opposite of a quench. In a quench, the temperature is lowered abruptly, and in a burn, the temperature is raised abruptly.

IV. SIMULATION RESULTS

A. Quenches from the disordered state

We first perform three quenches from the disordered state ($k_BT/J=2k_BT_c/J$) into the tube ($k_BT/J=4.25$), the capsule ($k_BT/J=3.75$), and the plug state ($k_BT/J=3.2$) (none of these is shown). We find that, in all three cases, the system forms a tube, because the surface field $H_1/J=0.7$ is too strong. The time required for the appearance of small domains, namely plugs or capsules, is far longer than the time required to create a metastable wetting layer and to squeeze the nonwetting phase into a tube. This is a somewhat artificial result, because for a more realistic model with longer-ranged interactions between spins, the time required for the formation of small domains is reduced [45]. In a real system, the system may therefore form small domains rather than a metastable tube for wetting forces of comparable strength. In order to obtain small domains upon a deep quench from the disordered phase within our model, we reduced the strength of the surface field significantly. Figure 3 shows stages in the spinodal decomposition from the disordered state $k_BT/J=2k_BT_c/J$ into the plug state at $k_BT/J=3.2$, for a surface field $H_1=0.1J$, at five different times following the quench. As expected, the domain growth slows down dramatically once the plugs are formed. As shown in Figs. 3(d) and 3(e), there is no perceptible domain growth between 310 000 and 470 000 MCS.

Recent cell-dynamical simulations performed by Marko on spinodal decomposition near a planar wall [46] are consistent with the above observations of the formation of the metastable wetting layer. The planar wall simulations demonstrate that there are three main factors controlling the time scale for the formation of the wetting layer after a quench from the single-phase region. These are the structure of the initial state, the thermal noise driving spinodal decomposition in the final state, and the strength of the surface field [46]. In the case of a pore, it is more difficult to prevent the wetting layer from forming first because the surface to volume ratio is higher. In our case, the initial state is nearly homogeneous, and the quench depth is fixed by the wetting and interfacial shape-transition temperatures. Therefore, we can prevent the formation of the wetting layer only by reducing the surface field.

B. Tube breakup kinetics

We first demonstrate the hysteresis at the interfacial shape transition predicted in the phenomenological theory. We begin with seven equally spaced and equally sized plugs equilibrated at $k_BT/J=3.2$, whose lengths are equal to the pore diameter. At time $t=0$ the temperature of the plugs is raised to $k_BT/J=4.4$, well above the interfacial shape transition. We find that the plugs rapidly coalesce into a tube within $t=25\,000$ MCS (not shown here). Next, we perform the reverse quench: we begin with a tube equilibrated at $k_BT/J=4.25$, and quench into the plug state at $k_BT/J=3.25$. The breakup of the tube into plugs is shown in Fig. 4. The pictures show that the tube first breaks up by pinching off at one point after about 525 000 MCS. Thus, it takes much longer for the tube to break up into plugs than for the plugs to coalesce into a tube. This is consistent with the observations on quenching from $T>T_c^0$ into the plug phase, where the system first formed a metastable tube instead of plugs at this value of the surface field ($H_1/J=0.7$).

We now study the breakup of the tube as a function of quench depth. We quench the tube at $k_BT/J=4.25$ into the capsule regime, at $k_BT/J=3.75$. The time sequence is not shown here, but we find that the tube again pinches off at one point after about 500 000 MCS.

It is difficult to establish whether we see evidence of a "spinodal line" for the tube. The pinching-off event that we observe occurs at only one point along the tube, so it should probably be described as a nucleation event. A close examination of Fig. 4, however, shows that after 525 000 MCS, the tube is definitely rippled in a roughly periodic way. Although the ripples do not grow in amplitude to the point where the tube breaks up, they may be evidence that the system is approaching the spinodal line. At later times, two more pinching-off events occur, leading to a series of three small plugs of roughly equal size, rather than one large plug. Thus our observations could be interpreted as evidence for an incipient instability of the tube.

C. Domain-growth kinetics

Let us now examine the growth kinetics of capsules, focusing on the dependence of the growth rate on temperature. In the next series of runs, we begin with seven equilibrated small plugs, whose lengths are equal to the pore diameter. In each run, we begin at the same initial temperature, at $k_BT/J=3.2$, and perform a single burn. The magnitude of the burn is varied in each run. First, we perform a small burn; we raise the temperature of the plugs at time $t=0$ to $k_BT/J=3.55$, just above the wetting transition. Figure 5 displays the resulting magnetization profiles at four times following the burn. In the

second run, we heat the plugs at $t=0$ to $k_BT/J=3.75$, midway between the wetting and interfacial shape transition. Figure 6 shows the profiles at four times following the burn. At this higher temperature, the kinetics are noticeably faster than those shown in Fig. 5. At $k_BT/J=3.55$ (Fig. 5), it takes 300 000 MCS for the initial seven capsules to coalesce into four capsules. At $k_BT/J=3.75$ (Fig. 6), it takes only 100 000 MCS for the seven capsules to coalesce into a single capsule. Finally, in the third run, we heat the plugs to $k_BT/J=3.85$, closer to the interfacial shape transition. The results are displayed in Fig. 7 for four times following the burn. At this temperature, the seven capsules coalesce into a tube in roughly 70 000 MCS, much faster than in the two previous runs.

The sensitivity of the growth rate to temperature appears consistent with the predictions of the phenomenological theory. According to the theory, however, the capsules coalesce by moving towards each other by diffusion. In Figs. 5–7, it is clear that none of the capsules moves as a unit as a function of time. On the time scale of the simulations, the diffusion of an entire capsule is apparently irrelevant. Rather, the capsules appear to coalesce owing to interactions between the endcap interfaces. As the temperature is increased, the interaction range also increases, presumably leading to faster coalescence.

The runs in Figs. 6 and 7 also illustrate other effects. In Fig. 6, the capsule formed after 100 000 MCS eventually breaks into two smaller capsules, due to internal tensile stresses. These stresses arise because the capsule is stretched beyond its equilibrium length, which is determined by the equilibrium wetting-layer thickness and the total volume of the capsule. Evidently, diffusion through the wetting layer is still slow enough so that the capsule breaks up before it has time to shrink to its equilibrium length.

Figure 7 illustrates the effect of the nearby first-order interfacial shape transition on the kinetics. As discussed above, the initial seven capsules quickly coalesce into a tube. The important feature here is that the tube is metastable at this temperature. Thus the system is trapped in a metastable configuration. The time required to reach the true capsule equilibrium state is drastically increased, because the system must now wait for a nucleation event. Such an event is shown in Fig. 7, where the tube pinches into two capsules after 1 080 000 MCS.

The last point in this section concerns the effect of initial domain size on growth kinetics. As mentioned above, an array of seven small plugs heated into the tube state coalesces into a tube in a remarkably short time. We believe that the coalescence time is short because the range of interactions between interfaces is roughly comparable to the distance between them. We are, however, also interested in the effect of diffusion through the wetting layer on the coalescence time. In order to reduce the effect of interfacial interactions, and to study the diffusion specifically, we start with a *single* plug, and heat into the tube state. In this case, somewhat surprisingly, the system becomes trapped in a metastable capsule state. In the first 250 000 MCS, the plug grows into a longer capsule. For the next 250 000 MCS, the capsule oscillates in length by stretching and shrinking. Finally, the capsule grows to some "critical" length, beyond which it grows monotonically into a tube, after roughly 2×10^6 MCS. This final slow growth from the capsule to the tube is probably due to the diffusion of the wetting layer along the entire length of the capsule, which is about three-quarters of the pore length. Thus, we do observe the effect of diffusion through the wetting layer on the growth rate.

V. SUMMARY OF SIMULATION RESULTS

In these simulations, we have studied two phenomena associated with the kinetics of phase separation in small pores. The first is the kinetics of the breakup of the tube configuration, when quenched into the capsule or plug regime. The second is the growth kinetics of capsules and plugs. According to a phenomenological model [14], the breakup kinetics of the tube should show two distinct behaviors, depending on the quench depth. For shallow quenches, there should be an energy barrier between the tube and capsule configurations, and the tube should break up by nucleation, pinching off at a single point along its length. For deep quenches, there should be no energy barrier, and the tube should break up via an instability, pinching off at periodic intervals along its length. In our simulations, the tube always pinches off at a single point first, rather than at several points simultaneously. Thus we always observe breakup by nucleation. However, in the deeper quenches, the tube radius appears to vary periodically along its length (see Fig. 4), perhaps indicating an incipient instability. For very deep quenches, the kinetics are extremely slow. We suspect that the instability of the tube occurs at quench depths too large for the kinetics to be observable, for this value of the surface field.

The second phenomenon studied here is associated with the growth kinetics of capsules and plugs. We observe that the growth kinetics of domains slows down dramatically when the domain size becomes comparable to the pore radius. This is in part due to the quasi-one-dimensional nature of the geometry, which inhibits Ostwald ripening. However, the simulations also show an extremely strong dependence of the coarsening rate on temperature. When the temperature is higher, the interactions between interfaces are longer in range, presumably leading to faster domain growth. We have also shown that the growth rate depends strongly on the domain size, as expected.

The growth rate is also influenced by the proximity of the first-order interfacial shape transition at k_BT_i/J. When we heat a set of several plugs to just *below* k_BT_i/J, the system tends to get trapped in a metastable tube state [47]. When we heat a single plug to just *above* k_BT_i/J, the system is trapped in a metastable capsule state. On the other hand, if we heat the set of plugs to just above k_BT_i/J, or a single plug to just below k_BT_i/J, we observe *no* metastability. Thus, the behavior we observe depends on the initial configuration as well as the final temperature after the burn.

In conclusion, the simulations exhibit many features predicted by the phenomenological theory, but from very different mechanisms. For example, in our simulations, the strong dependence of domain growth on temperature appears to arise from the range of interfacial interactions; in our hydrodynamic calculations, on the other hand, it arises from the sensitivity of flow to the wetting-layer thickness. In a real system, hydrodynamic flow, diffusion, and interfacial interactions all play a role. We find that the effect of all of these factors is to slow down the kinetics dramatically as the temperature is lowered further into the two-phase region.

Finally, we address the usefulness of macroscopic descriptions in describing behavior in small pores. The simulations of Liu and Grest [15] showed that macroscopic ideas are extremely successful in predicting the wetting-phase behavior in small pores. In these simulations, we again do not see any behavior that cannot be explained qualitatively using macroscopic ideas; interactions between interfaces can easily be incorporated in a macroscopic description. Thus our results indicate that macroscopic descriptions are surprisingly successful in describing phase-separation kinetics in pores on the scale of a few tens of angstroms.

ACKNOWLEDGMENTS

We are grateful to D. S. Cannell, M. H. W. Chan, S. B. Dierker, B. J. Frisken, W. I. Goldberg, J. S. Huang, M. Y. Lin, S. K. Sinha, P. Wiltzius, and X.-l. Wu for numerous discussions of their experiments. In particular, M. Y. Lin and S. K. Sinha provided plots of their data and data analysis before publication. This work was supported in part by the Camille and Henry Dreyfus Foundation.

APPENDIX A: TUBE BREAKUP KINETICS: SPINODAL LINE

When the tube configuration is quenched into the capsule or plug phases, the tube can either pinch off to form a single capsule or plug, or it can undergo an instability and pinch off to form a series of capsules or plugs. The former process is similar to nucleation and the latter process is analogous to spinodal decomposition. In a previous paper, Liu *et al.* [14] provided an incorrect expression for the position of the spinodal line in the phase diagram. We stress that the error makes no qualitative difference in the wetting-phase diagram, and does not alter the physical picture presented in Ref. [14]. Here, we show the correct derivation of the spinodal line. As in Ref. [14], we begin by constructing the free energies per unit length of the capsule and tube configurations. These are given by

$$f_{\rm cap}=2\pi\varphi_\beta r_0^2[\sigma+\overline{A}V(r_c)]/r_c \ , \tag{A1}$$

where $f_{\rm cap}$ is the free energy of the capsule phase, φ_β is the volume fraction occupied by the β phase ($\varphi_\beta=\frac{1}{2}$ corresponds to critical composition), r_0 is the pore radius, r_c is the capsule radius, σ is the $\alpha\beta$ interfacial tension, $\overline{A}$ is the Hamaker constant, and $V(r)$ is the effective interface potential for two concentric cylinders of radius r and r_0. In this expression, we have neglected the contribution of the end caps of the capsule to the free energy; thus (A1) is valid when the pore dimensions satisfy $L\gg r_0$. The capsule radius r_c is found by minimizing (A1) and solving

$$\sigma+\overline{A}[V(r_c)-r_cV'(r_c)]=0 \ . \tag{A2}$$

The free energy of the tube phase is given by (A1) with r_c replaced by the tube radius

$$r_t=\sqrt{\varphi_\beta r_0} \ . \tag{A3}$$

Thus, the free energy of the tube phase is

$$f_{\rm tube}=2\pi r_t[\sigma+\overline{A}V(r_t)] \ . \tag{A4}$$

Given the free energy of the tube configuration, we can calculate the position of the spinodal line in the phase diagram. The free energy of an arbitrary axisymmetric surface is

$$F=2\pi\int dz\ \Sigma(r(z))r(z)\left[1+\left[\frac{dr}{dz}\right]^2\right]^{1/2} , \tag{A5}$$

where the "effective surface tension" $\Sigma(r)$ is given by

$$\Sigma(r)=\sigma+\overline{A}V(r) \ . \tag{A6}$$

The volume of the enclosed surface, which is held constant owing to the composition constraint, is

$$V=\pi\varphi_\beta r_0^2L=\pi r_t^2L=\pi\int dz\,[r(z)]^2 \ . \tag{A7}$$

If we set $r(z)=r_1+\epsilon r_t\sin qz$, where $\epsilon\ll 1$, then we can solve for r_1 in terms of r_t and ϵ using (A7). Assume that $L=2\pi n/q$, where n is an integer. Then

$$r_1=r_t(1-\tfrac{1}{2}\epsilon^2)^{1/2}\simeq r_t(1-\tfrac{1}{4}\epsilon^2) \tag{A8}$$

and

$$r(z)=r_t(1+\epsilon\sin qz-\tfrac{1}{4}\epsilon^2) \ . \tag{A9}$$

Now expand the expression for F around r_t to second order in ϵ to obtain

$$F/L=f_{\rm tube}+\tfrac{1}{2}\pi\epsilon^2r_t[r_t^2\Delta(r_t)+q^2r_t^2\Sigma(r_t)] \ , \tag{A10}$$

where

$$\Delta(r)=\overline{A}V''(r)+\overline{A}V'(r)/r-[\sigma+\overline{A}V(r)]/r^2 \tag{A11}$$

and $f_{\rm tube}$ is given by (A4).

From (A10), we see that the free energy F/L is always higher than the unperturbed tube free energy $f_{\rm tube}$ if $\Delta>0$; thus, in this case, the tube is stable against perturbations. If $\Delta<0$ is satisfied, however, then the tube is unstable to long-wavelength perturbations, and will break up. Thus the position of the spinodal line is given by

$$\Delta=0 \ . \tag{A12}$$

Finally, the expression (A11) should be compared to the incorrect form given in Eq. (5) in Ref. [14]:

$$\Delta=\overline{A}V''(r)-\sigma/r^2 \ . \tag{A13}$$

This error does not lead to any qualitative differences in the phase diagram.

APPENDIX B: TUBE BREAKUP KINETICS: LINEAR STABILITY ANALYSIS

From the linear stability analysis, we can determine the wavelength of the fastest growing mode, to obtain an estimate of the resulting capsule or plug size. One of the ingredients of the calculation is the Laplace pressure, or the pressure drop across the $\alpha\beta$ interface. In the absence of a wetting potential, the pressure difference is given by

$$p_\beta - p_\alpha = \sigma(c_1 + c_2) , \tag{B1}$$

where c_1 and c_2 are the two principal radii of curvature of the interface. In the presence of a wetting potential, the expression for the Laplace pressure is modified [48]:

$$p_\beta - p_\alpha = \Sigma(r)(c_1 + c_2) + \Sigma'(r) , \tag{B2}$$

where $\Sigma(r)$ is given by (A6). In Ref. [14], the following expression for the Laplace pressure was used:

$$p_\beta - p_\alpha = \sigma(c_1 + c_2) + \Sigma'(r) . \tag{B3}$$

This led to errors in Eqs. (5) and (6) in Ref. [14]. As noted in Appendix A, this error makes no qualitative difference in the phase diagram.

Before embarking on the linear stability analysis, we define several dimensionless variables. We introduce a time $\tau \equiv \eta_\beta r_0/\sigma$, where η_β is the viscosity of the β phase. Then we define the following dimensionless variables: the radial distance $R = r/r_0$, the axial distance $x = z/r_0$, time $t = T/\tau$, the fluid velocities in the two phases $u_i = v_i \tau/r_0$, the fluid pressures in the two phases $p_i = P_i r_0/\sigma$, and the viscosity ratio $\eta = \eta_\alpha/\eta_\beta$. We denote the interface position at position x by $\rho(x)$, and define the volumetric flux of each phase:

$$Q_\alpha = 2\pi \int_\rho^1 u_\alpha R \, dR \tag{B4}$$

and

$$Q_\beta = 2\pi \int_0^\rho u_\beta R \, dR . \tag{B5}$$

We then have a set of three equations to solve. The first is the Navier-Stokes equation. We assume that the Reynolds number is low and that the lubrication approximation holds, so all of the flow is in the axial direction:

$$\eta_i \frac{1}{R} \frac{d}{dR} \left[R \frac{du_i}{dR} \right] = \frac{dp_i}{dx} . \tag{B6}$$

The second equation states that there is no net fluid flow:

$$Q_\alpha + Q_\beta = 0 ; \tag{B7}$$

and the third equation is the continuity equation for the volumetric flux of β:

$$\frac{\partial}{\partial t}(\pi \rho^2) = \frac{\partial}{\partial x} Q_\beta . \tag{B8}$$

We also need boundary conditions for the Navier-Stokes equation. We use no-slip conditions at the pore surface

$$u_\alpha(R = 1) = 0 , \tag{B9a}$$

zero-slope conditions at the pore center

$$\left. \frac{du_\beta}{dR} \right|_{R=0} = 0 , \tag{B9b}$$

matched velocities at the interface

$$u_\alpha(R = \rho) = u_\beta(R = \rho) , \tag{B9c}$$

and matched stresses at the interface

$$\eta \left. \frac{du_\alpha}{dR} \right|_{R=\rho} = \left. \frac{du_\beta}{dR} \right|_{R=\rho} . \tag{B9d}$$

Finally, we have expression (B2) recast in dimensionless units:

$$p_\beta - p_\alpha = \frac{1}{\sigma} \left[\Sigma(\rho) \left[\frac{1}{\rho} - \frac{d^2\rho}{dx^2} \right] + \Sigma'(\rho) \right] . \tag{B10}$$

The remainder of the calculation is straightforward. We solve (B6) to find

$$u_i = \frac{1}{4\eta_i} R^2 \frac{dp_i}{dx} + c_0^i \ln R + c_1^i , \tag{B11}$$

where the four constants c_0^i and c_1^i are determined in terms of dp_α/dx and dp_β/dx by matching to the boundary conditions (B9a). Since the difference of the pressures is given by (B10), the four constants can be written in terms of dp_β/dx alone. We substitute the solutions (B11) into the definition of the volumetric fluxes (B4) and (B5). We can then use (B7) to solve for dp_β/dx. We find

$$\frac{dp_\beta}{dx} = \frac{d(p_\beta - p_\alpha)}{dx} \frac{(1-\rho^2)^2}{\rho^4(1-\eta) - 1} . \tag{B12}$$

We put this expression into the equation for Q_β and substitute into the continuity equation (B8). Finally, we use

$$\rho(x) = \rho_t + \rho_1 e^{iqx + \omega t} \tag{B13}$$

and linearize (B8) in $\rho_1 \ll \rho_t$ to obtain the dispersion relation. In real units, this is

$$\omega = \frac{a_0 \sigma}{16 r_t \eta_\alpha} q^2 [\Delta(r_t) - q^2 \Sigma(r_t)] , \tag{B14}$$

where Δ is given by (A11) and a_0 is a function of ρ_t:

$$a_0 = (1 - 3\rho_t^2)(1 - \rho_t^2) - 4\rho_t^4 \ln \rho_t + \frac{(1-\rho_t^2)^4}{\rho_t^4(1-\eta) - 1} . \tag{B15}$$

We find that a_0 is always positive. For the case of critical composition, the tube radius is $\rho_t = 1/\sqrt{2}$. If we assume that the viscosities of the two components of the binary liquid mixture are nearly the same, then the viscosity ratio satisfies $\eta \simeq 1$ near the critical point, and $a_0 \simeq 0.034$. Note that the quantity enclosed in square brackets in (B14) is identical to the result obtained in the energetic calculation.

Given the dispersion relation (B14), we can obtain the

wavelength of the fastest growing mode:

$$\lambda = 2\pi r_0 (\Delta/2\Sigma)^{1/2} . \quad \text{(B16)}$$

Not surprisingly, the length scale is set by the pore radius r_0.

APPENDIX C: DOMAIN GROWTH KINETICS—HYDRODYNAMIC CALCULATIONS

The earlier paper, Ref. [14], quoted results for the diffusion constant of capsules. The calculation is sketched here. We begin with a capsule of dimensions $r = \rho r_0$ and l, with $r \ll l$ so that we can neglect the capsule end caps. The diffusion constant of the capsule is given by the Stokes-Einstein relation

$$D = k_B T/\Lambda , \quad \text{(C1)}$$

where Λ is the drag on the capsule. But Λ is given by

$$F_{\rm av} = \Lambda u_{\rm av} , \quad \text{(C2)}$$

where $F_{\rm av}$ is an average force on the capsule and $u_{\rm av}$ is its resulting average velocity. In Appendix B we applied an average force given by

$$F_{\rm av} = \pi r^2 l \frac{d(p_\beta - p_\alpha)}{dx} , \quad \text{(C3a)}$$

and obtained a resulting average velocity

$$u_{\rm av} = \left[2\pi \int_0^\rho u_\beta R \, dR \right] \Big/ (\pi\rho^2) . \quad \text{(C3b)}$$

The resulting expression for the drag is

$$\Lambda = 8\pi l \eta_\alpha \rho^2 / H(\rho) , \quad \text{(C4)}$$

where

$$H(\rho) = 2(\rho^2 - 1) - 4\rho^2 \ln\rho + [2 - \rho^2(2-\eta)](1-\rho^2)^2/[1-\rho^4(1-\eta)] . \quad \text{(C5)}$$

In the limit $\rho \to 1$, when the wetting layer grows very thin, we find, for $\eta = 1$,

$$H(\rho) = 10(1-\rho)^2 + O((1-\rho)^3) . \quad \text{(C6)}$$

Thus the diffusion constant in that limit is

$$D = \frac{5 k_B T (1-\rho)^2}{4\pi \eta_\alpha \rho^2 l} . \quad \text{(C7)}$$

The capsule diffuses more slowly as the wetting layer thins, owing to the factor of $(1-\rho)^2$. It also diffuses more slowly as its length increases, owing to the factor of l in the denominator. Finally, note that the results quoted in Ref. [14] for the diffusion constant and coalescence times are correct; the errors in the expressions for $F_{\rm av}$ and $u_{\rm av}$ cancel in the calculation of the drag.

[1] M. C. Goh, W. I. Goldburg, and C. M. Knobler, Phys. Rev. Lett. **58**, 1008 (1987); W. I. Goldburg, in *Physics of Complex and Supermolecular Fluids*, edited by S. A. Safran and N. A. Clark (Wiley, New York, 1987), p. 475.

[2] S. B. Dierker and P. Wiltzius, Phys. Rev. Lett. **58**, 1865 (1987).

[3] P. Wiltzius, S. B. Dierker, and B. S. Dennis, Phys. Rev. Lett. **62**, 804 (1989).

[4] S. B. Dierker, B. S. Dennis, and P. Wiltzius, J. Chem. Phys. **92**, 1320 (1990).

[5] S. B. Dierker and P. Wiltzius, Phys. Rev. Lett. **66**, 1185 (1991).

[6] M. Y. Lin, S. K. Sinha, J. M. Drake, X.-l. Wu, and P. Thiyagarajan (unpublished).

[7] F. Brochard and P. G. de Gennes, J. Phys. Lett. (Paris) **44**, 785 (1983).

[8] P. G. de Gennes, J. Phys. Chem. **88**, 6469 (1984).

[9] D. Andelman and J. F. Joanny, in *Scaling Phenomena in Disordered Systems*, edited by R. Pynn and A. Skjeltorp (Plenum, New York, 1985).

[10] D. A. Huse, Phys. Rev. B **36**, 5383 (1987).

[11] A. Maritan, M. R. Swift, M. Cieplak, M. H. W. Chan, M. W. Cole, and J. R. Banavar, Phys. Rev. Lett. **67**, 1821 (1991).

[12] M. R. Swift, M. Cieplak, A. Maritan, N. Shrimpton, W. J. Ma, and J. R. Banavar (unpublished).

[13] R. J. Birgeneau, R. A. Cowley, G. Shirane, and H. Yoshizawa, J. Stat. Phys. **34**, 817 (1986).

[14] A. J. Liu, D. J. Durian, E. Herbolzheimer, and S. A. Safran, Phys. Rev. Lett. **65**, 1897 (1990).

[15] A. J. Liu and G. S. Grest, Phys. Rev. A **44**, 7879 (1991).

[16] P. Levitz and J. M. Drake, Phys. Rev. Lett. **58**, 686 (1987); P. Levitz, G. Ehret, S. K. Sinha, and J. M. Drake, J. Chem. Phys. **95**, 6151 (1991).

[17] R. Vacher, T. Woignier, J. Pelous, and E. Courtens, Phys. Rev. B **37**, 6500 (1988).

[18] F. Ferri, B. J. Frisken, and D. S. Cannell, Phys. Rev. Lett. **67**, 3626 (1991).

[19] A. P. Y. Wong and M. H. W. Chan, Phys. Rev. Lett. **65**, 2567 (1990). Wong and Chan study vapor-liquid ^{4}He in aerogels, and find a narrow coexistence curve with an exponent consistent with the three-dimensional Ising value of $\beta \sim \frac{1}{3}$.

[20] B. J. Frisken, F. Ferri, and D. S. Cannell, Phys. Rev. Lett. **66**, 2754 (1991).

[21] B. J. Frisken and D. S. Cannell (unpublished).

[22] A. P. Y. Wong, S. B. Kim, J. Ma, W. I. Goldburg, and M. H. W. Chan (unpublished).

[23] See, e.g., R. Evans, U. Marini Bettolo Marconi, and P. Tarazona, J. Chem. Phys. **84**, 2376 (1986); B. K. Peterson, K. E. Gubbins, G. S. Heffelfinger, U. Marini Bettolo Marconi, and F. van Swol, J. Chem. Phys. **88**, 6487 (1988), and references therein.

[24] M. W. Cole and W. F. Saam, Phys. Rev. Lett. **32**, 985 (1974); Phys. Rev. B **11**, 1086 (1975).

[25] S. J. Gregg and K. S. W. Sing, *Adsorption, Surface Area and Porosity* (Academic, New York, 1967).

[26] D. D. Awschalom, J. Warnock, and M. W. Shafer, Phys. Rev. Lett. **57**, 1607 (1986).

[27] A. P. Y. Wong, Ph.D. dissertation, Pennsylvania State University, 1990.

[28] R. Bruinsma, in *Hydrodynamics of Disperse Media*, edited by J. P. Hulin, A. M. Cazabat, E. Guyon, and F. Carmona (Elsevier, New York, 1990).

[29] S. B. Dierker and P. Wiltzius (private communication).
[30] A. J. Liu and M. E. Fisher, Physica A **156**, 35 (1989).
[31] H. Nakanishi and M. E. Fisher, Phys. Rev. Lett. **49**, 1565 (1982).
[32] C. Ebner, W. F. Saam, and A. K. Sen, Phys. Rev. B **32**, 1558 (1985); C. Ebner and W. F. Saam, Phys. Rev. Lett. **58**, 587 (1987).
[33] D. E. Sullivan and M. M. Telo da Gama, in *Fluid Interfacial Phenomena*, edited by C. A. Croxton (Wiley, New York, 1986), p. 45.
[34] D. B. Abraham, N. M. Svrakic, and P. J. Upton, Phys. Rev. Lett. **68**, 423 (1992).
[35] H. Nakanishi and M. E. Fisher, J. Chem. Phys. **78**, 3279 (1983); M. E. Fisher and H. Nakanishi, J. Chem. Phys. **75**, 5857 (1981).
[36] A. O. Parry and R. Evans, Phys. Rev. Lett. **64**, 439 (1990); Phys. Rev. Lett. **66**, 2175 (1991).
[37] M. R. Swift, A. L. Owczarek, and J. O. Indekeu, Europhys. Lett. **14**, 475 (1991); J. O. Indekeu, A. L. Owczarek, and M. R. Swift, Phys. Rev. Lett. **66**, 2174 (1991).
[38] J. C. Lee (unpublished).
[39] A. Chakrabarti (unpublished).
[40] E. Pytte, Y. Imry, and D. Mukamel, Phys. Rev. Lett. **43**, 808 (1979).
[41] In fact, DW used this form at all temperatures. Below T_c^0, they found that the amplitude of the Lorentzian-squared term is small, as expected. Both DW and Lin *et al.*, however, see the extra peak even below T_c^0; this may be due to an adsorption layer.
[42] P. Debye, H. R. Anderson, and H. Brumberger, J. Appl. Phys. **28**, 679 (1957).
[43] S. K. Sinha (private communication).
[44] J. D. Gunton, M. San Miguel, and P. S. Sahni, in *Phase Transitions and Critical Phenomena*, edited by C. Domb and M. S. Green (Academic, New York, 1983), Vol. 8.
[45] M. Laradji, M. Grant, M. J. Zuckermann, and W. Klein, Phys. Rev. B **41**, 4646 (1990).
[46] J. F. Marko (private communication).
[47] Note that it may be easier to observe the tube configuration experimentally because of the tendency of the system to be trapped in the metastable tube state.
[48] We do not derive the expression here, but the procedure is outlined in L. D. Landau and E. M. Lifshitz, *Statistical Physics*, 3rd ed. (Pergamon, New York, 1980), Part I, pp. 522–524.

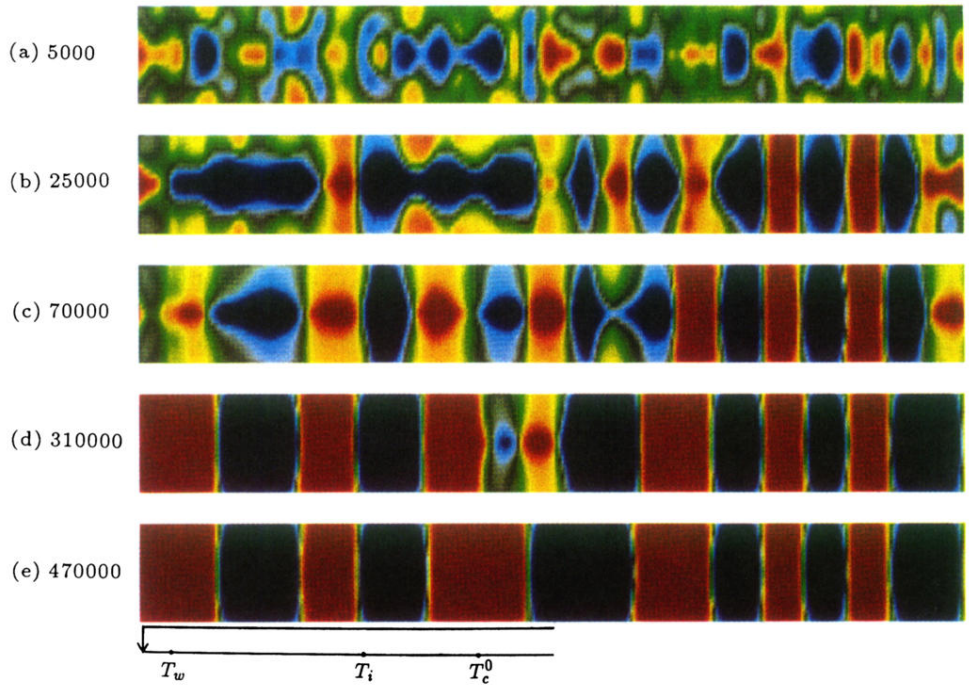

FIG. 3. Spinodal decomposition in a pore. We quench from the disordered phase ($k_B T/J = 2k_B T_c/J$) into the plug phase ($k_B T/J = 3.2$) at time $t = 0$. The surface coupling is $J_1/J = 1.0$, the bulk field is $H/J = 0$, and the surface field is $H_1/J = 0.1$. Magnetization profiles are shown at the times indicated on the left. The surface field is extremely low so the contact angle in (e) is nearly 90°. Note that the domain growth slows down once the domain size becomes comparable to the pore radius. These profiles were obtained by averaging over 20 000 MCS.

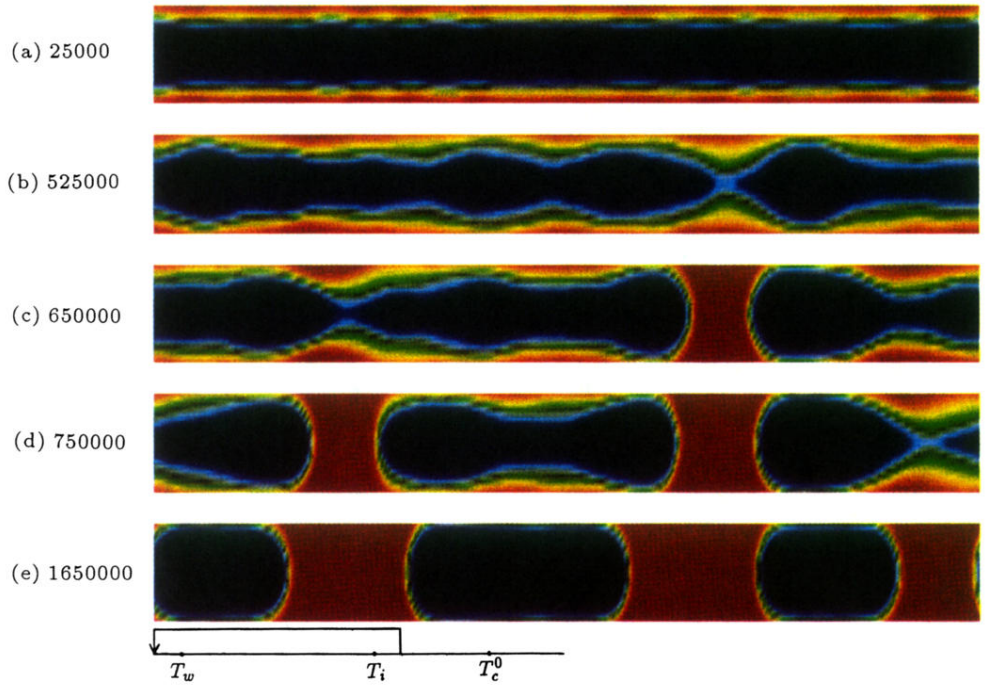

FIG. 4. Tube breakup kinetics. We quench from the tube phase ($k_B T/J = 4.25$) into the plug phase ($k_B T/J = 3.25$). The parameters $J_1/J = 1.0$, $H/J = 0$, and $H_1/J = 0.7$ are used. Times are indicated on the left. Note that the tube pinches off first at one point, so it breaks up via nucleation. However, it eventually pinches off at two more points, to form three nearly equal-sized plugs, which one would expect if it had broken up via an instability ("spinodal decomposition"). Thus the evidence for the existence of a "spinodal line" is inconclusive. The profiles were obtained by averaging over 25 000 MCS.

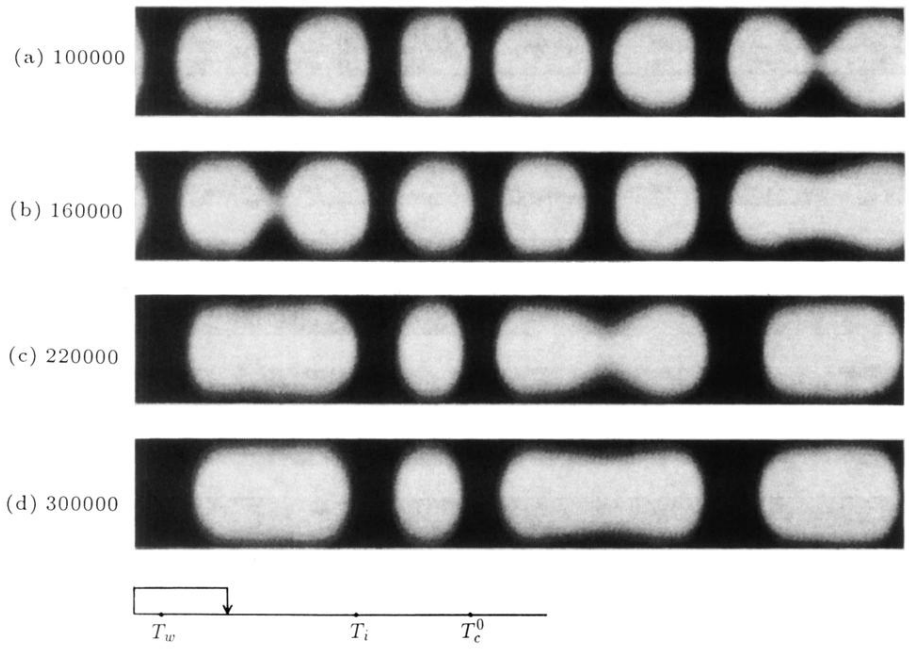

FIG. 5. Domain-growth kinetics. We heat from the plug phase ($k_B T/J = 3.2$) into the capsule phase ($k_B T/J = 3.55$) just above the wetting transition at time $t = 0$. We use $J_1/J = 1$, $H/J = 0$, and $H_1/J = 0.7$. The wetting layer forms quickly after the burn [see (a)], but the capsules grow extremely slowly, apparently because the interaction between interfaces is short-ranged compared to the spacing. See Figs. 6 and 7 for comparison of growth rates. Profiles were averaged over 10 000 MCS.

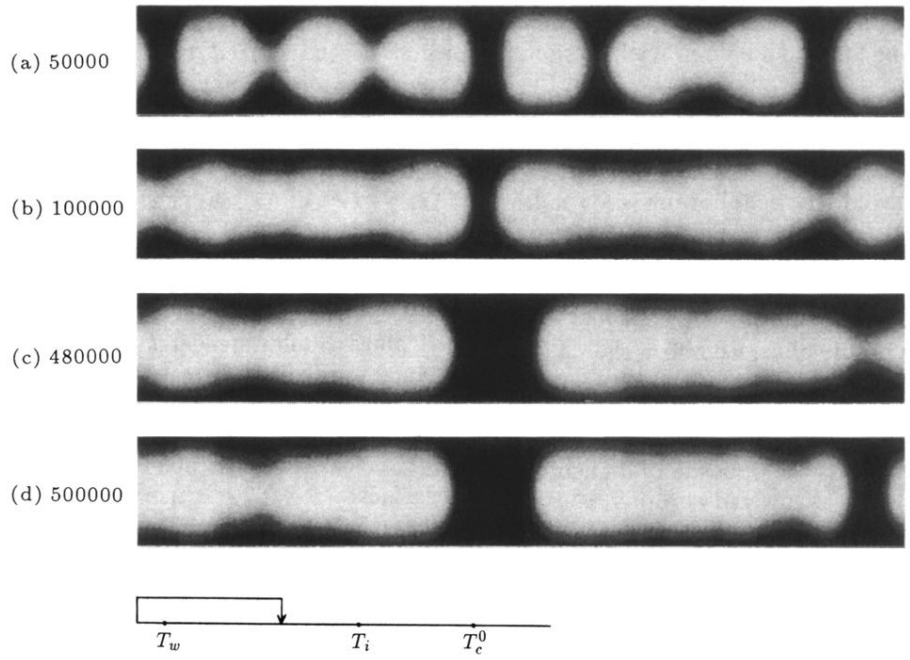

FIG. 6. Domain-growth kinetics. We heat from the plug phase ($k_B T/J = 3.2$) to roughly the midpoint of the capsule phase ($k_B T/J = 3.75$) at $t = 0$. The coupling constants and fields are the same as in Fig. 5. The wetting layer is thicker than in Fig. 5, and the kinetics of capsule coalescence are noticeably faster. Profiles were averaged over 10 000 MCS.

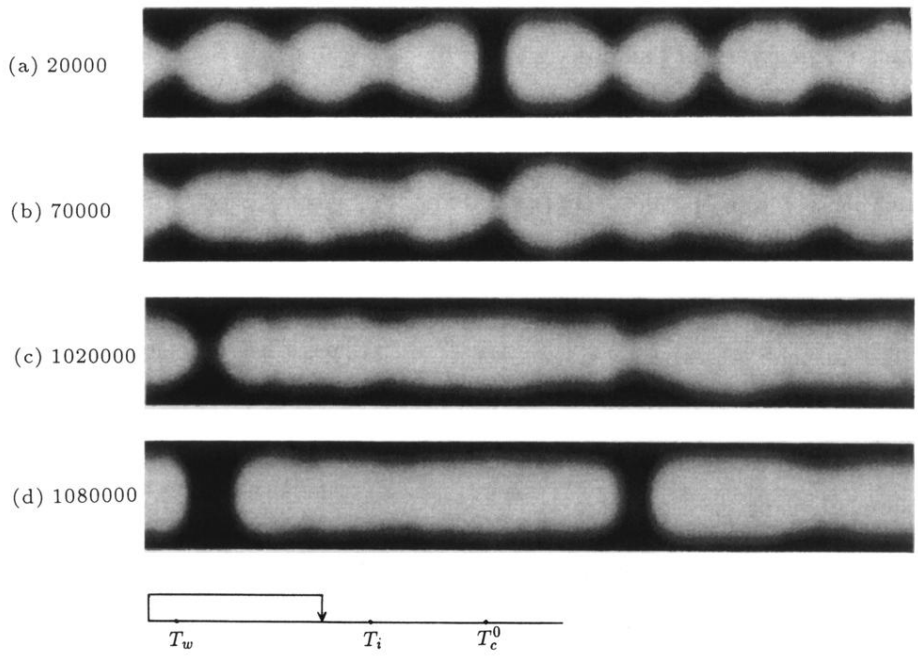

FIG. 7. Domain-growth kinetics. We heat from the plug phase ($k_B T/J = 3.2$) into the capsule phase ($k_B T/J = 3.85$) just below the interfacial shape transition. The coupling constants and fields are the same as in Fig. 5. The capsules coalesce rapidly [see (a)]. The influence of the nearby interfacial shape transition is apparent; the system is trapped in the metastable tube, and cannot reach the equilibrium capsule configuration until a nucleation event occurs [see (c)]. Profiles were averaged over 30 000 MCS.